Carlos III University

Boundary layer mitigation by means of plasma actuators

by

Lorena del Amo Martin

Supervised by

Yacine Babou, Oscar Flores

A thesis submitted for the
Degree of Aerospace Engineering

in the
Leganes Technical College
Aerospace Engineering Department

September 2015

Acknowledgements

This work started in the Aerospace Engineering Department with my two supervisors Yacine Babou and Oscar Flores. I would like to express my gratitude to both professors for encouraging me to select the topic of this present paper as Final Thesis of the Degree.

I would like to offer my special thanks to Yacine Babou for initiating me in the investigation labour and teaching me not only theoretical knowledge about the topic, but also to develop new skills as student. I am particularly grateful for his full availability to help me out anytime, even in the summer days or Sunday evenings.

Furthermore, I wish to acknowledge the help provided by Oscar Flores and Pablo Fajardo in all the Fluent simulation carried out with fluent. Thanks for their dedication and effort, and for their quick answers to any particular doubt during the time of this work.

Finally, thanks to my family and friends that have supported me since the beginning of this work, facilitating the investigation labor and encouraging me the whole adventure.

Contents

List of Figures

List of Tables

Abbreviations

AC	**A**lternate **C**urrent
CFD	**C**omputational **F**luid **D**ynamics
DBD	**D**ielectric **B**arrier **D**ischarge
EHD	**E**lectro **H**ydrodimanic **D**ynamic
MAV	**U**ser **A**rial **V**ehicle
RF	**R**adio **F**requency
SDBD	**S**urface **D**ielectric **B**arrier **D**ischarge
UAV	**U**nnamed **A**rial **V**ehicle
UDF	**U**ser **D**efine **F**unction

Chapter 1

Introduction

Boundary layer control has led to several discussions within the aerodynamic scope. Many related issues regarding flow separation are of interest due to its detrimental consequences. Well-known associated problems such as buffet have to do with this phenomenon. Nevertheless, flow control extents not only to airfoil flow control but also to any airflow in general such as internal aerodynamics (ducts or diffusers), internal and external blades or other flying bodies, UAV and MAV, among others.

Todays methods for airfoil boundary layer control can be divided in two main categories of solutions. The first category corresponds to the group that gathers passive methods, whereas the second category deals with active methods, like flapping wings or methods based on Micro Electro Mechanical Systems and Electrohydronamic Actuators (EHD), which transform electrical into mechanical power. These kind of actuators built on this principle are the so-called plasma actuators, ranging from corona discharges and electric barrier discharges (DBDs), glow discharges and arc discharges.

The most employed active controls in the Aeronautical Industry are typically parts integrated into the airfoil, modifying the lifting surface. The moving mechanical parts are known as flaps and slats. Moving parts are the main cause of vibrational and acoustic problems, such as control reversals, divergence or flutter; severe aeroeleastic problems associated to the controls of the lifting surfaces.

An alternative to moving mechanisms is the use of active controls based on plasma actuators, which have been tremendously investigated during the last decade. Plasma actuators demonstrate their potential for flow control at the leading edge or centre of

the airfoil, inducing significant the attachment and detachment of the boundary layer, without the addition of mechanical parts. The application of DBD on other bodies such as cylinders have led to the suppression of the global instability and the vortex shedding for different Reynolds range.

Several experimental tests have been performed over these bodies with smoke visualizations providing a better physical understanding of the plasma effect on boundary layer mitigation [2] [3]. The reader is encouraged to see the addressed references in the literature.

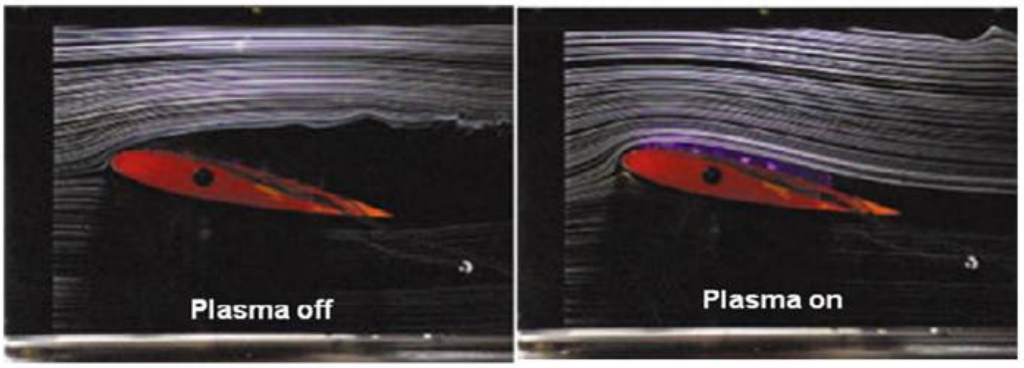

FIGURE 1.1: Plasma actuator over an airfoil

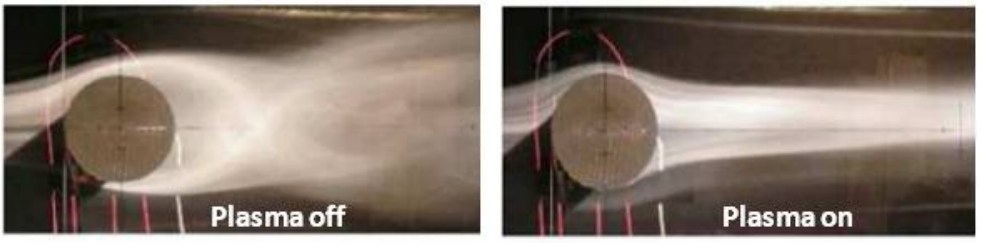

FIGURE 1.2: Plasma actuator over a cylinder

As a rule, a plasma actuator is a simple device skinned in Figure 1.3. Generally, it is composed of two electrodes, one exposed to air and one encapsulated, integrated in a dielectric material, and finally, the Surface Dielectric Barrier Discharge (SDBD), or plasma, that is created in the upper surface of the dielectric, namely, the purple colored area. The configurations of plasma actuators may vary from symmetric to non-symmetric according to the disposition of the two electrodes, parallel or opposed configurations, among others.

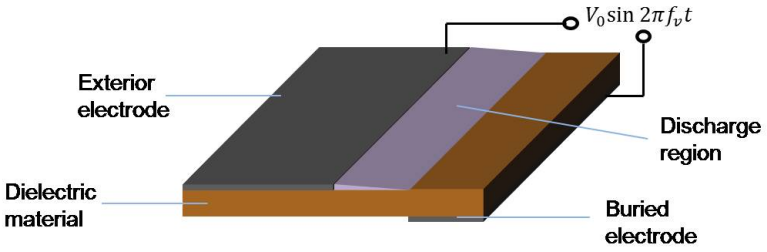

FIGURE 1.3: SDBD configuration

Plasma airflow actuation mechanism is based on momentum transfer to the surrounding air by means of collisions of the produced ions during the electrical discharges (plasma) with the surrounding air particles. The result is an electrodynamic force, thrust, that pushes the fluid in the neighborhood of the discharged region.

The advantages of Plasma Actuators for airflow control are the suppression of moving mechanical parts and the high time response. Several experiments, [4], have shown its efficient performance to reattachment at high angles of attack; yet, limited by the Reynolds number. Besides, the cost of the setting is low due to the easy schematic and the materials required that lead to an easy manufacturing.

Surface Dielectric Barrier Discharge (SDBD), or plasma, is a complex medium containing neutral spices electron and ion interaction through collision and with a self-consistent electric field. Because the prediction of the thrust generated by a DBD and its effect on airflow is far from trivial (necessity of coupling the Navier-Stokes equations with Poisson equations and the kinematics) for systematic calculations, it is better to model the effect of the DBD actuator in a simple body source term that can be easily implemented into commercial CFD solver. With this simple model, engineers can play with the source term for the study of the aerodynamic performance of different applications, such as boundary control.

All in all, the primary objective of this paper is to represent the thrust generated by a surface dielectric barrier discharge (SDBD) in a new force model form, in order to implement it in a CFD solver, as it is the case of Fluent. The heritage of this paper is two main studies where the distribution of the force of a plasma actuator is approximated, and a second one, where the absolute value of the thrust of plasma actuators has been calculated.

Starting from scratch, this paper is divided in different chapters. Initially the state of the art and the selected geometry of the plasma actuator is specifically defined, followed by the description of the two models of interest that are the bases to build the new model of force. Once the third model of force is built, a preliminary assessment on a CFD solver, Fluent, will be performed for the three addressed models. The numerical assessment has been the main task of the project in order to provide an accurate simulation of the velocity vector profiles and velocity magnitude for the force models, lasting two months for the developments of all the calculations. Finally, analysis of the results is gathered at the end.

Two-dimensional modeling is assumed to be a good approach for all the forces, as long as, it perfectly allows the simulation of the SDBD evolution, as well as, the simplifications in calculations that it entails. The work is modeled to a mechanical point of view, neglecting the complexity of the physics of the plasma, yet with a formulation compliant with the plasma physics.

Chapter 2

SDBD models of force

2.1 Description of the model

The typical configuration of the plasma actuator that we consider in the present study is hereafter represented by Figure 2.1. The setting, as previously mentioned, is composed by two electrodes, one exposed to air, and one encapsulated, integrated in a dielectric material referred as the lower electrode. An alternate voltage is applied between the two electrodes, of typical magnitude of 10 kV with a frequency of 10 kHz.

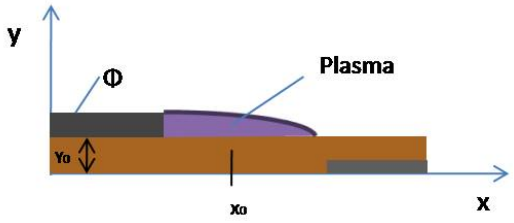

FIGURE 2.1: Asymmetric SDBD schematic

The above schematic represents an asymmetric single dielectric barrier plasma actuator, where x_0 is the mid position between the two electrodes and y_0 the thickness of the dielectric material, also called d in the followings, with a typical value lower than 1 mm up to 5 mm. The relative dielectric constant of the dielectric material is denoted as ε , typically a value of between 2 and 6. The thickness of the electrodes is considered to be negligible. Assuming that the lower electrode is encapsulated, plasma is generated in the upper part of the dielectric material, the discharge region, with length extension l , typically of the same length as the gap between the two electrodes.

Rigorously, the momentum transfer from the plasma to the surrounding air is due to the acceleration of ions in both directions depending on the applied voltage. The generation of thrust with DBD plasma actuator is a complex phenomena that involves momentum transfers at microscopic scale that can be schematized as following:

The electron accelerated in the electric field dissociate and ionize the neutral species of air (O2, N2), then positive ions are accelerated in the electric field and collides with neutral species (which are insensitive to the electric field), and transfers their kinetic energy through individual collisions leading to the generation of directed thrust observable at macroscopic scale.

For the proper modeling of plasma actuators, continuity equations need to be solved for different species, Poissons Equation, and Navier-Stokes equations self-consistently. Previous studies solving these equations have lead to different formulations (see [1], Section I. This procedure is a time consuming task and rather expensive.

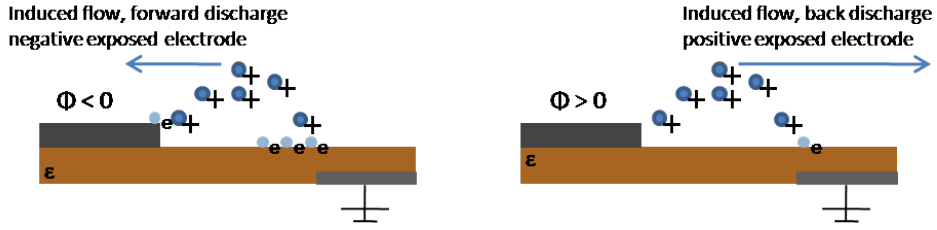

FIGURE 2.2: Momentum tranfer

From an engineering point of view, the generated thrust can be approximated as a steady momentum force, where a thrust pushes the air in one direction, depending on the configuration of the actuator, which for the schematic in 2.1. pushes the fluid to the right. In this way, the plasma physics are reduced to a mechanical problem, effective for the methodology of this study. In the followings, the plasma actuator is operating in atmospheric air.

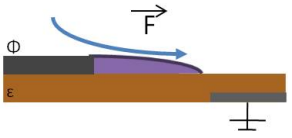

FIGURE 2.3: Steady thrust approximation

Focusing on the methodologies of this work, the heritage of this study is two approximated models of force: the global thrust model by by V R Soloviev [5] and local

thrust model by Singh et al. [1]. The former model predicts the total amount of generated thrust by the actuator [5] whereas the latter describes the local thrust density distribution generated by the actuator.

Each model will be explained in the forthcoming sections and the third model will be built at the end on the bases of the two addressed models.

2.2 Global thrust model

V R Soloviev [5] has recently obtained an analytical estimation of the integral value of the body force (thrust) of a SDBD. His main driver to work on it was the understanding of the saturation effect that is produced in the actuator. Additionally, the expression obtained by V R Soloviev provides a direct relation between the voltage parameter and the dielectric material properties on the performance of the plasma actuator.

The integration of the body force over space and its averaging over time, give thrust per unit electrode length equal to:

$$Thrust = \frac{1}{TV}\int_0^{Tv}\int_{-\infty}^{-\infty}\int_0^{\infty} f(t,x,y)dtdxdy \tag{2.1}$$

Where TV is the period of the applied voltage.

By substituting and integrating this last expression the final thrust generated by SDBD is retrieved. Nevertheless, a thorough substitution of the value of each parameter that composes the integral is carried out in [5]. The final expression is showed and hereafter plotted.

$$T_{sol} = 2.4 \times 10^{-10}{\alpha_l}^4 \frac{fV(cm)}{d(kHz)}\left(\frac{9V_0}{4\Delta V_c}\right)^4\left(1-\frac{7\Delta V_c}{6V_0}\right)^4\left(1-exp\left(-\frac{1}{4f_v\Delta\tau_q}\right)\right) \tag{2.2}$$

Where $\alpha_l = 1, \Delta V_c = 0.6kV, \Delta\tau_q = 100 \times 10^{-6}$ seconds, values taken from [5], following his recommendations. Moreover f_V is the frequency, d corresponds to the thickness of the material and V_0 is the voltage applied.

For different dielectric materials with variable thickness and frequencies, Figure 2.5 shows the behavior of Equation 2.2. The predicted force dependencies match qualitatively the experimental results gathered in [5], Section 3.5: Estimation of thrust.

Material	d(cm)	fV(kHz)	ε
Teflon	0.635	2.1	2
Derlin	0.635	2.3	3.5
Quartz	0.635	2.3	4.2
Teflon	0.318	2	2
Macor	0.318	2.3	6
Kapton	0.015	4.4	3.9

TABLE 2.1: Material properties

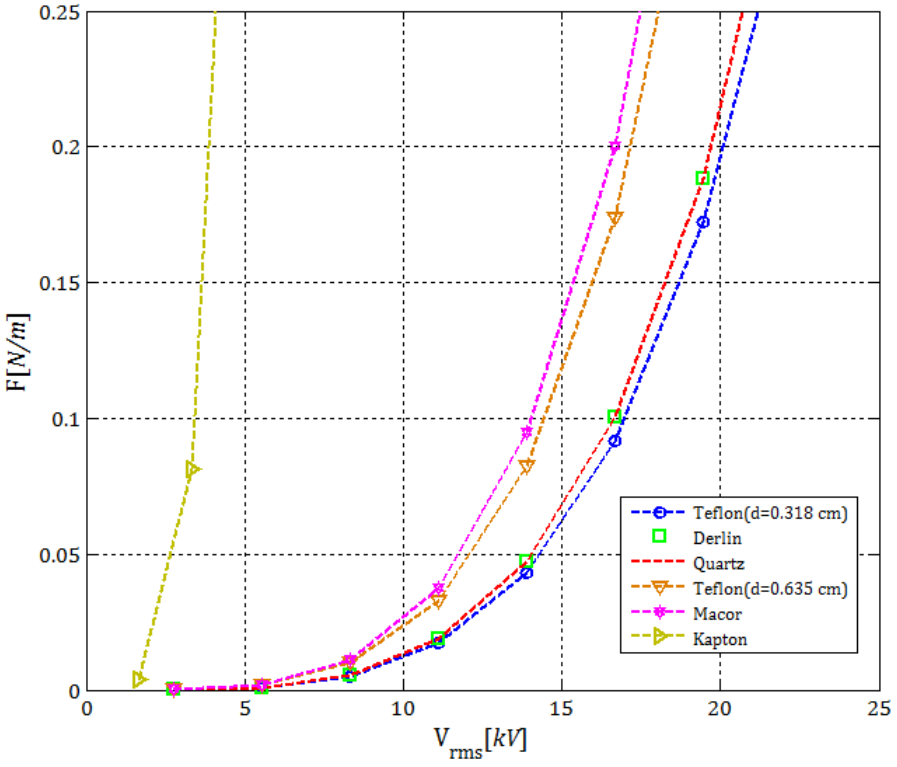

FIGURE 2.4: Theoretical estimation of Thrust per unit electrode length for different dielectric materials and variable dielectric thickness ($V_{rms} = V_0/1.7$)

2.3 Local thrust model

Kunwar Pal Singh et al. [1] approximated the spatial dependence of the EHD force for calculations in air. The approximated force is a fourth order polynomial of applied RF voltage built for the asymmetric schematic defined at the beginning of this chapter, Figure 2.1.

An asymmetric dielectric barrier discharge model is presented for real gas air chemistry using a self-consistent multibody system of plasma, dielectric, and neutral gas modelled together to predict the electrodynamic force imparted to the working gas.

After performing the whole calculation, Equation 2.3 is the final approximated distribution of the Electrodynamic force generated by a plasma actuator derived by [1],

$$\begin{aligned}\vec{f}(x,y) = F_{x_0} V_0^4 \exp\left\{-\left(\frac{x - x_0 - (y - y_0)}{y}\right)^2 - \beta_x (y - y_0)^2\right\}\vec{i} \\ + F_{y_0} V_0^4 \exp\left\{-\left(\frac{(x - x_0)}{y}\right)^2 - \beta_y (y - y_0)^2\right\}\vec{j}\end{aligned} \tag{2.3}$$

Where F_{x_0} and F_{y_0} are the averaged value of the electrodynamic force obtained by solving air-plasma equations. x_0 is the midpoint between the rf and the grounded electrode, and y_0 corresponds to the thickness of the dielectric material (Figure 2.1). β_x and β_y are function of the dielectric material and have been selected so as to match the velocity induced by the electrodynamic force. V_0 corresponds to the voltage applied.

The approximated force, Equation 2.3, is hereafter plotted and reproduced in order to understand the behavior, shape of the force and the value of it at the boundaries of the domain Figures 2.6. The rest of the values elected so as to solve 2.3 were, $F_{x_0} = 2.6$, $F_{y_0} = 2.0$, $x_0 = 0.015$ m, $y_0 = 0.001$ m, $\beta_x = 8 \times 10^5$, $\beta_y = 10^7$.

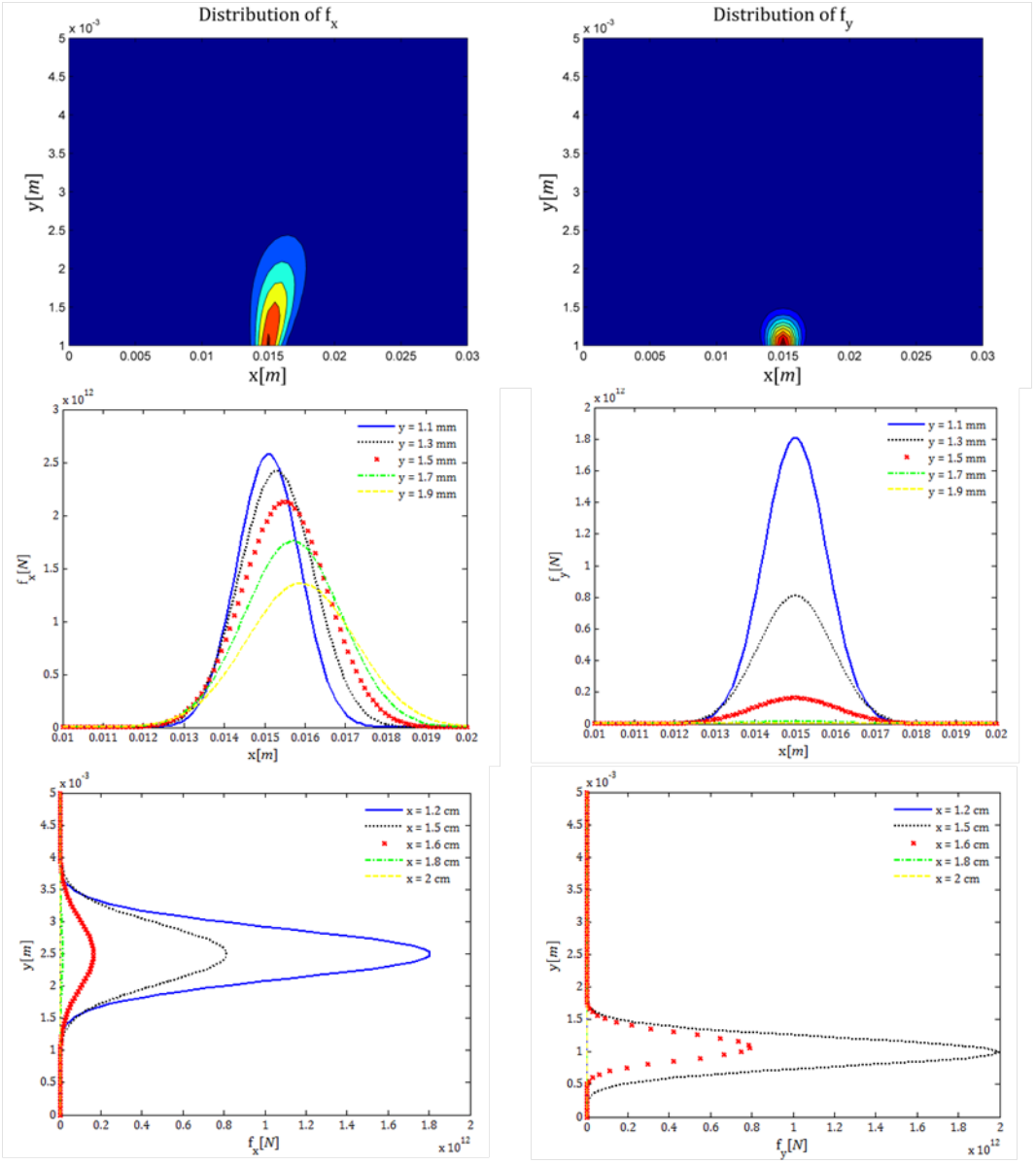

FIGURE 2.5: 2D and XY plots of the distributed force. Left figures for the Fx component and right figures for Fy component of the force.

The force is concentrated in the reference point of the actuator, for the plotted figures at 0.015 m in the x-axis, tending to zero for the limits of the domain. According to this, the pressure at those limits is equal to the ambient pressure. The air is stationary, quiescent, with density of 1.225 Kg/m3.

2.4 Thrust-Voltage force model

This third point is the core of this paper and a future tool for flow control based on plasma actuators. Once the two previous models have been defined and understood, the next step is to merge them together for a proper formulation of the new force model. *

The advantages of this new force model is a key step for obtaining a more generic model capable of predicting the performance of the SDBD on air.

To that end, the local thrust model needs to be normalized.

This task starts by calculating the integral of the distributed force, expression 2.4, in order to normalize this integral to unity. The resulting integral expression is given hereafter,

$$\begin{aligned}\vec{F} = \iint F_{x_0} \exp\Big\{-\Big(\frac{x - x_0 - (y - y_0)}{y}\Big)^2 - \beta_x (y - y_0)^2\Big\}\vec{i} \\ + \quad F_{y_0} \exp\Big\{-\Big(\frac{(x - x_0)}{y}\Big)^2 - \beta_y (y - y_0)^2\Big\}\vec{j} \quad dxdy\end{aligned} \tag{2.4}$$

It was a non-trivial computation that needed to be performed thoroughly. For more information about the integral procedure and the normalization process see Appendix A.

After making the integral and normalization of the distributed force, the final step left is to multiply it with the absolute value of the force retrieved by V R Soloviev, expression 2.2, leading to the following expression:

$$\vec{T_0} = T_{sol}\big(V, \varepsilon, d, fV\big) \times \frac{\vec{f}\big(F_{x0}, F_{y0}, \beta_x, \beta_y\big)}{\|\vec{F}\|} \tag{2.5}$$

Resulting into the final Equation A.9 from Appendix A,

$$\begin{aligned}\vec{T_0} = 2.4 \times 10^{-10} {\alpha_l}^4 \frac{f_v(cm)}{d(kHz)} \Big(\frac{9V_0}{4\Delta V_c}\Big)^4 \Big(1 - \frac{7\Delta V_c}{6V_0}\Big)^4 \Big(1 - exp\Big(-\frac{1}{4 f_v \Delta\tau_q}\Big)\Big) \\ \times \frac{1}{\|\vec{F}\|} \times \Big[r \times \exp\Big\{-\Big(\frac{x - x_0 - (y - y_0)}{y}\Big)^2 - \beta_x (y - y_0)^2\Big\}\vec{i} \\ + \exp\Big\{-\Big(\frac{(x - x_0)}{y}\Big)^2 - \beta_y (y - y_0)^2\Big\}\vec{j}\Big]\end{aligned} \tag{2.6}$$

Clearly, the advantages of this new model outweigh the disadvantages of the other two, as it is the combination of both in order to provide an improved version. The new expression of force depends only on the voltage applied, the dielectric material, and thickness of the dielectric material, and frequency which allows an easy configuration and parametric study.

$$F(V, \varepsilon, d, fV)$$

On the other hand, the integral expression still contains two more variables coming from the local thrust model, $\beta_x, \beta_y, F_{x_0}, F_{y_0}$. The last two terms appear also in form of a ratio, namely, r :

$$r = \frac{F_{x_0}}{F_{y_0}} \tag{2.7}$$

Figures 2.6 and 2.7, show the sensibility of β_x and β_y , to the value of the integral for each component of the force affected, that is, β_x on the effect of F_{x_0} and β_y for F_{y_0} . Besides, it can be easily told the effect on the integral value $(F_{x_0} = 2.6, F_{y0} = 2)$, as its directly proportional to it.

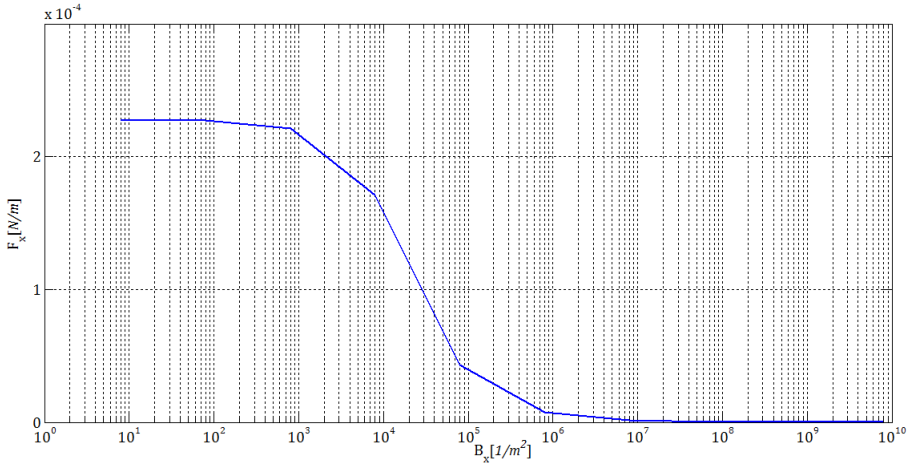

FIGURE 2.6: Effect of β_x on F_{x_0}

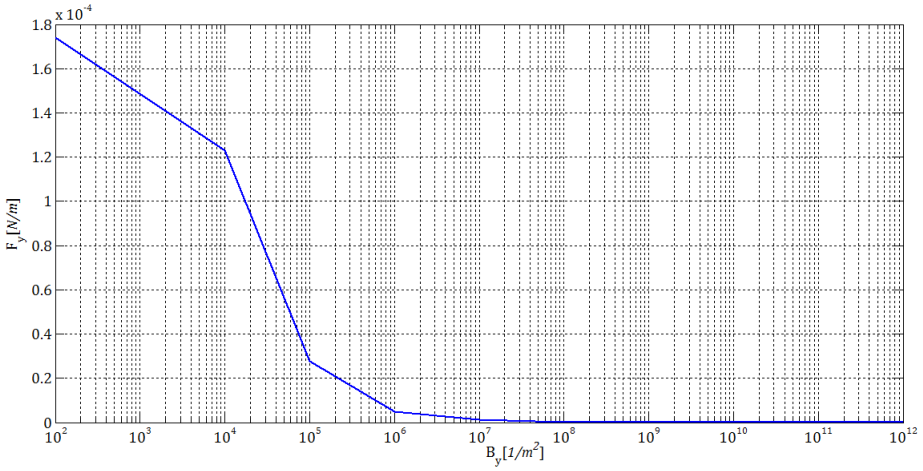

FIGURE 2.7: Effect of β_y on F_{y_0}

Lets remember that β_x and β_y are function of the dielectric material and have been selected so as to match the velocity induced by the electrodynamic force. For $\beta_x < 8 \times 10^5$ and $\beta_y < 10^7$ the value of the integrated force increases, whereas it decreases for $\beta_x > 8 \times 10^5$ and $\beta_y > 10^7$.

Following Singh et al. recommendations, the discussed values of $\beta_x, \beta_y, F_{x_0}, F_{y_0}$ are set to the reference proposed in [1], with:

F_{x_0} =2.6

$F_{y0} = 2$

$\beta_x = 8 \times 10^5$

$\beta_y = 10^7$

Chapter 3

Assessment in CFD solver: Fluent

3.1 Fluent framework

Computational Fluid Dynamics programs have the characteristic of solving Naiver-Stokes equations for any kind of fluid flow in a quantitative version of the results, namely, a numerical solution. The great advantage of CFD is that they can handle any kind of continuity, momentum and energy equation for several problems limited for the analytical scope.

The working principle of CFD is that the continuity, momentum, and energy equations are discretized. In order to do so, the flow domain is divided into a number of discrete points. A grid is generated and the discrete points are converted into grid points. There are many basis for dicretization, however, the basic principle is showed below, where the scripts of the grid points are defined:

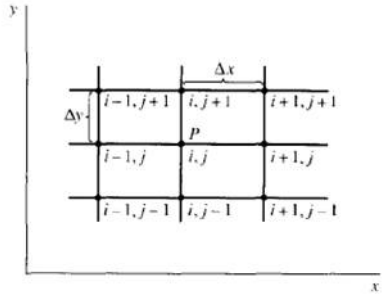

FIGURE 3.1: Grid points

For any differential or integral form, the equations are substituted and calculated iteratively for each point by means of substituting the points with the subscripts. For more information about the discretization process see [6], Chapter 2, section 17.

For the purpose of this paper, Fluent has been the computational software selected due to its availability at the Aerospace Engineering Department of Carlos III University. Fluent, among other features, allows the direct implementation of a source term in the Navier-Stokes momentum equations.

As regarded in Chapter 2, three models of force have been addressed; models, that indeed, need to be implemented in the momentum equations in order to solve the interactions between the plasma physics and the quiescent air, which surrounds the plasma. From a mathematical point of view, the force models are implemented with an specific User Define Function (UDF), programed in C, into Fluent, adding the corresponding source term into the Navier-Sotkes Equations:

$$\frac{\partial \rho}{\partial t} + \frac{\partial (\rho u_i)}{\partial x_i} = 0 \tag{3.1}$$

$$\frac{\partial (\rho u_i)}{\partial t} + \frac{\partial (\rho u_i u_j)}{\partial x_j} = -\frac{\partial p}{\partial x_i} + \frac{\partial \tau_{ij}}{\partial x_j} + \rho f_i \tag{3.2}$$

$$\frac{\partial (\rho e)}{\partial t} + (\rho e + p)\frac{\partial u_i}{\partial x_i} = \frac{\partial (\tau_{ij} u_j)}{\partial x_i} + \rho f_i u_i + \frac{\partial (\dot{q}_i)}{\partial x_i} + r \tag{3.3}$$

In classic notation,

$$\vec{\nabla} \cdot (\rho \vec{u}) = 0 \tag{3.4}$$

$$\frac{\partial (\rho \vec{u})}{\partial t} + \vec{\nabla} \cdot \rho \vec{u} \otimes \vec{u} = -\vec{\nabla} p + \vec{\nabla} \cdot \bar{\bar{\tau}} + \rho \vec{f} \tag{3.5}$$

$$\frac{\partial (\rho e)}{\partial t} + \vec{\nabla} \cdot (\rho e + p)\vec{u} = \vec{\nabla} \cdot (\bar{\bar{\tau}} \cdot \vec{u}) + \rho \vec{f} \vec{u} + \vec{\nabla} \cdot \vec{q} + r \tag{3.6}$$

In the momentum equations, 3.2 and 3.5, the source terms are defined and implemented in the f_i or, in the classic notation, $\vec{f}$, components.

As far as the aim of this paper is concerned, a variety of simulations in Fluent of the models of force is performed in order to obtain the velocity vector profiles of the surrounding air when plasma is activated.

On top of that, the general Fluent methodology is hereafter introduced:

- **Preprocessing**

1. A geometry domain is set with the tool Design Modeler. The selected domain is a rectangular, two dimensional. The dimensions of the domain are 0.03 m long and 0.01 m high.

2. The fluid domain is divided into several cells. Several attempts were performed to finally obtain a quadratic and uniform mesh. The recommendation for the mess is to refine it, till the solution does not differ from the previous one. The final mess values considered are:

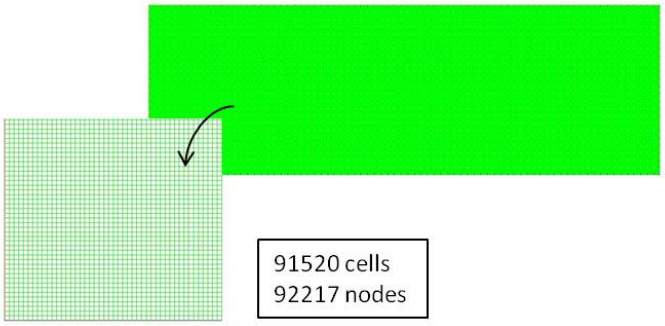

FIGURE 3.2: Mesh dimensions

Nevertheless, for some simulations additional refinement close to the lower wall was required depending on the distribution of the force.

3. Set of the boundary conditions. The boundary conditions for the domains are as follows: the left, right and upper limits are set to pressure outlet conditions, which entail setting the pressure of those limits to ambient pressure. The causes of selecting pressure-outlet are due to the force distributions, which is zero at the limits of the domain, so no moving air is expected at those values. Lastly, the lower boundary is considered as a non-slip wall, acting as the upper surface of the dielectric material.

- **Simulation**

It is configured to steady, non-viscous, Spalart-Allmaras turbulent model, quiescent air and the cell domain is defined with the three models of force, separately for each case.

Preliminary simulations were performed in laminar flow, with no success in terms of convergence of the solution. This led to the use of the Spalart-Allmaras model, which is a turbulent viscous model specifically recommended for wall-bounded flows. It is generally use for aerospace applications, and it worked for the simulations carried out in the current paper.

The simulation is solved iteratively till the solution is converged. After each iteration, the residual sum of each variable is calculated and stored, so it is created and recorded a convergence history, which can be visualized in the monitors.

- **Post-processing**

The post-processing allows displaying the results. Vectors, contours, XY plots are configured to visualize the outcome of the simulation.

3.2 Global thrust model assessment

Reproduction of the V. R. Soloviev, [5], global thrust model in a Fluent simulation is performed. To that end, arbitrary body force distributions are selected, on intuition of the local distribution of the EHD force. The two distributions are two Gaussian distributions and one rectangular distribution.

The arbitrary distributions times the thrust defined in Equation 2.2 is implemented in fluent. The total thrust selected for the calculation is 0.1 N/m, from the global thrust model, Figure 2.5.

a) 2D Gaussian distribution, of the form:

$$g(x,y) = A \times exp\Big[- \left(\frac{(x-x_0)^2}{2\sigma_x^2} + \frac{(y-y_0)^2}{2\sigma_y^2} \right) \Big] \tag{3.7}$$

where $x_0 = 0.015$ m and $y_0 = 0.001$ m. A is the normalization factor,

$$A = \frac{1}{\pi \sigma_x \sigma_y} \tag{3.8}$$

and σ_x and σ_y determine the shape to the Gaussian distribution. Two different sigma values, shapes of the Gaussian, are considered:

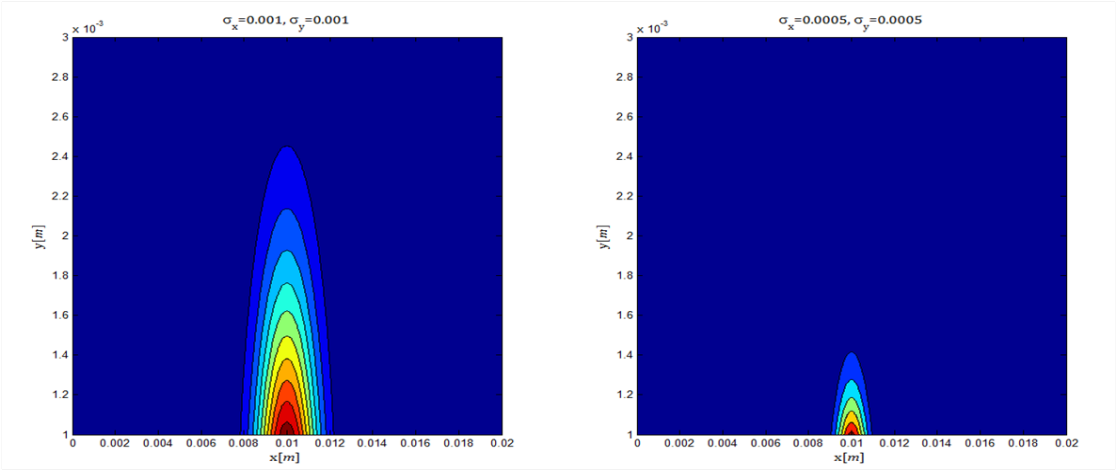

FIGURE 3.3: 2D Gaussian distribution. Left plot $\sigma_x = 0.001$, $\sigma_y = 0.001$ and right plot $\sigma_x = 0.0005$, $\sigma_y = 0.0005$

Velocity vectors and velocity vector profiles for Gaussian distributions are here after plotted. For the case of $\sigma_x = 0.001$, $\sigma_y = 0.001$, where the force density distribution is lower, smaller values of the velocity magnitude are retrieved. Meanwhile, for the second case, $\sigma_x = 0.0005$, $\sigma_y = 0.0005$, the velocity magnitude is higher. This is due to the fact that a decrease of the local distribution of the thrust, the surface, entails an increase of the total thrust, leading to an increase of the velocity magnitude profiles.

$\sigma_x = 0.001 \quad \sigma_y = 0.001$

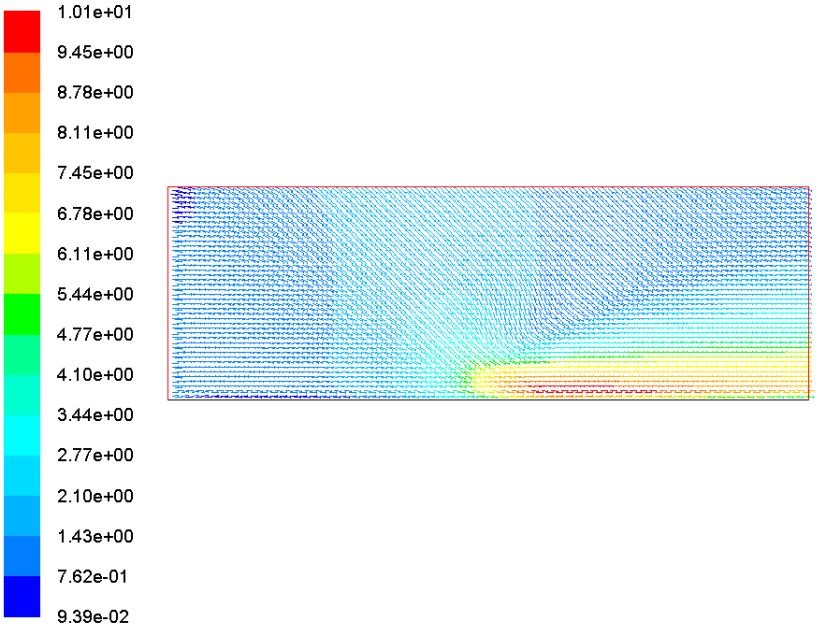

FIGURE 3.4: The velocity vectors for T= 0.01 N/m in m/s of the 2D Gaussian ($\sigma_x = 0.001$, $\sigma_y = 0.001$)

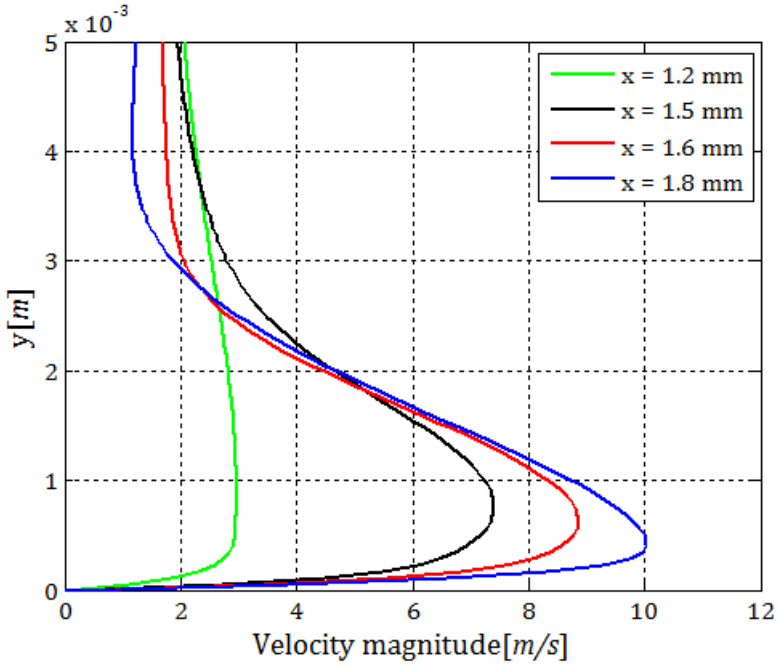

FIGURE 3.5: The velocity vector profiles for different x positions, as a function of y for T= 0.01 N/m (σ_x = 0.001 , σ_y = 0.001)

σ_x = 0.0005 σ_y = 0.0005

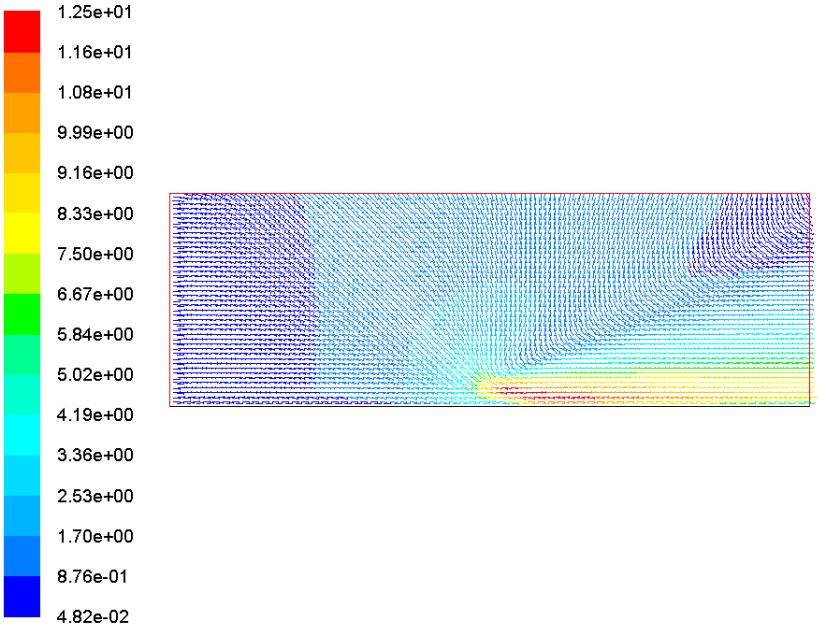

FIGURE 3.6: The velocity vectors for T= 0.01 N/m in m/s of the 2D Gaussian (σ_x = 0.0005 , σ_y = 0.0005)

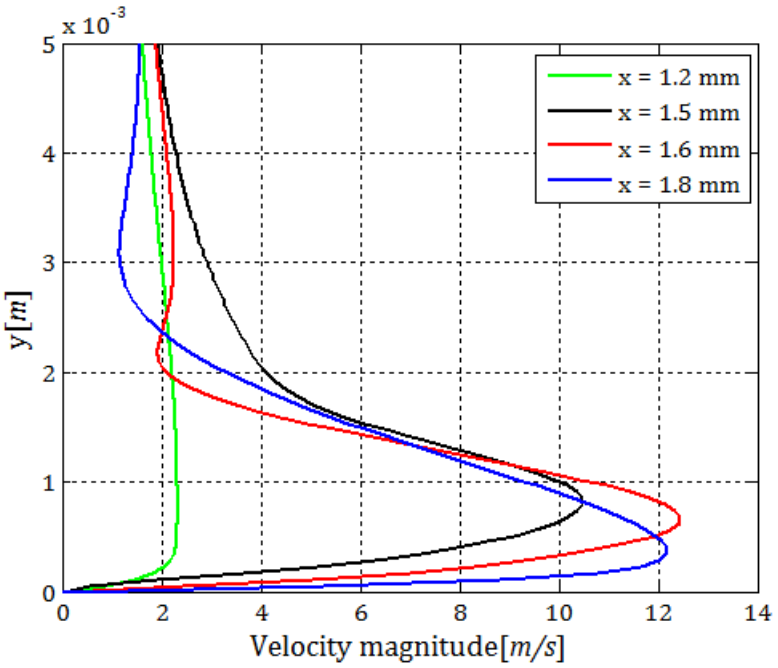

FIGURE 3.7: The velocity vector profiles for different x positions, as a function of y for T= 0.01 N/m (σ_x = 0.0005 , σ_y = 0.0005)

b) Rectangular distribution. It is located at the middle point of the domain, x=0.015 m, and on the lower wall boundary, at y= 0 m. The rectangle is 0.004 m long and 0.002 m high.

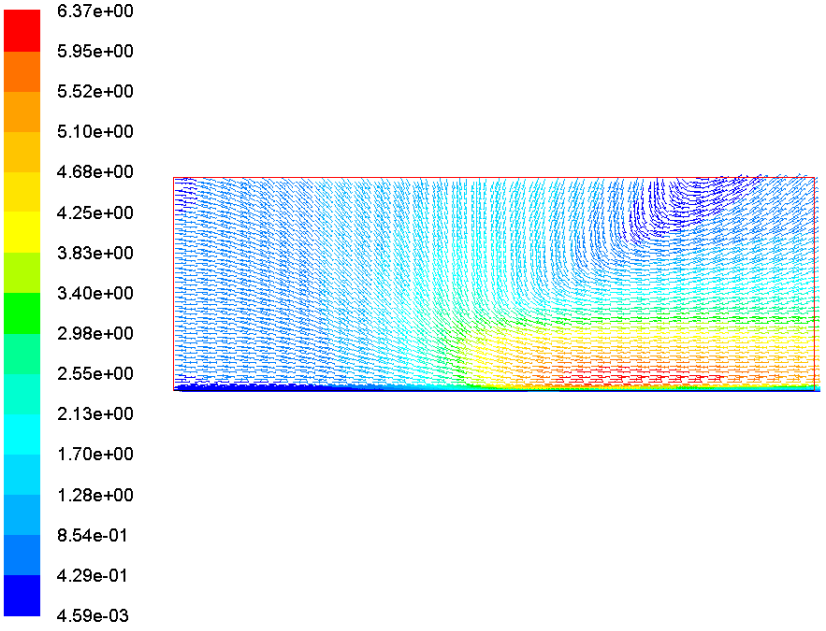

FIGURE 3.8: The velocity vectors for T= 0.01 N/m in m/s, of the rectangular distribution

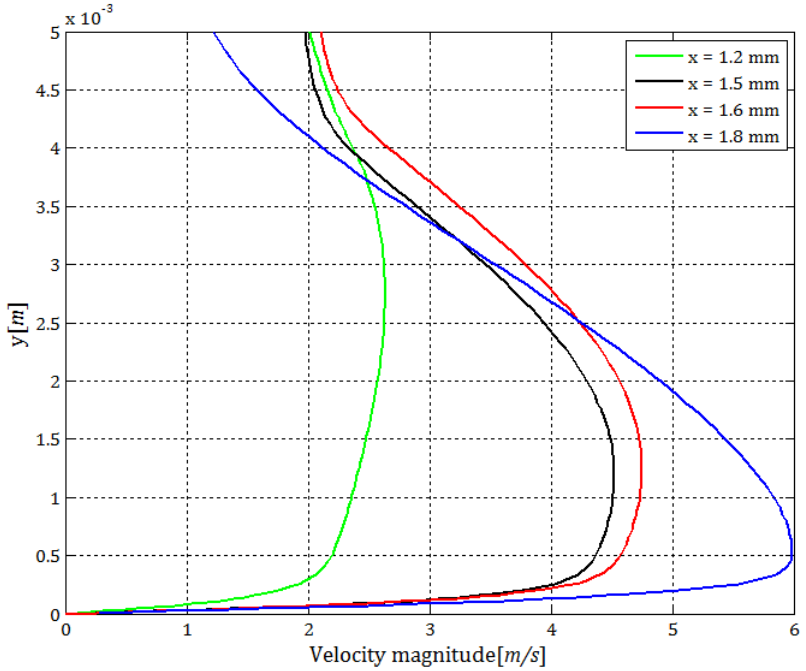

FIGURE 3.9: The velocity vector profiles for three x positions, as a function of y for T= 0.01 N/m, of the rectangular distribution

Comparing the velocity vector profiles of the rectangular distribution with those of the Gaussian distributions, it can be directly noticed that the resulting velocity profiles in terms of morphology are strongly different from the ones reproduced with the Gaussian. On the other hand, differences in the velocity magnitude can be found, yet with similar order of magnitude close to the experimental values for SDBD.

These results lead to an important fact that should be pointed out. The work reproduced by Soloviev [5] provides a valuable numerical estimation of the total thrust, however, there is no information about the distribution of the local EHD. Therefore, a model with the distribution of the local force is required in order to provide a complete force model. Otherwise, random distributions can be sketched following intuition. However, as we have shown for the square and the Gaussian distributions, the resulting velocity profiles can vary from 6 to 12 m/s.

The same remark can be done regarding the model of Singh [1] which predicts the distribution but does not predict the total thrust.

3.3 Local thrust model assessment

Results for a distributed force of the form, Equation 2.3, are showed after performing the simulation in Fluent and compared to the ones obtained by Singh et al. [1]. The chosen values of the parameters that compose the force are the same as defined in Chapter 2, Section 2.3.

As far as the voltage potential is concerned, it needs to be pointed out the high degree of proportionality in the force equation, as long as ϕ is elevated to the forth power. Any increase in the potential entails a sudden increase of the magnitude of the force. With the proposed values of [750 1000 1200] Volts, no convergence of the solution has been obtained during the Fluent simulations. In addition, the plots presented by Singh et al. [1] are normalized, so there is no quantitative sense of the values that are plotted.

Consequently, due to the lack of information regarding the scaling of the force (Equation 2.3), the final voltage potential is set to unity, so as to compare the shape and morphology of the force, leaving the actual scaling.

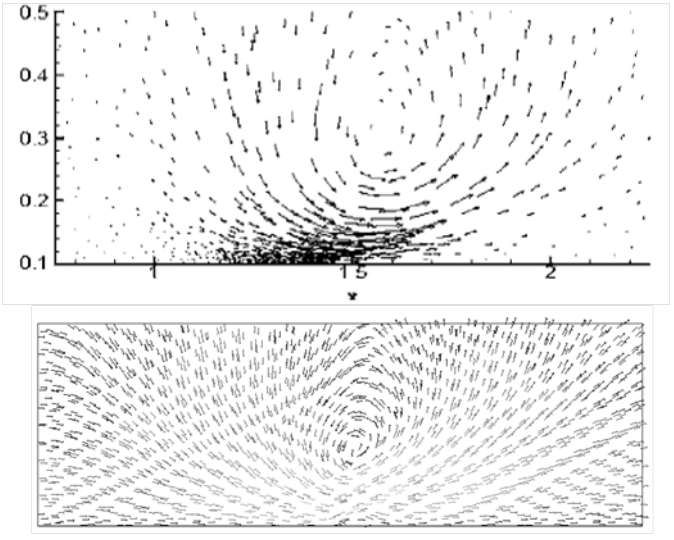

FIGURE 3.10: The velocity vectors of the local thrust model. In the upper plot velocity vectors for f =5 kHz and 1000 V retrieved in [1], lower plot velocity vectors for 1 V

In conclusion, despite the EHD force expression of Singh is not calibrated, there is agreement in terms of morphology and shape of the velocity profiles with retrieved by [1] and reported in the present paper. Fact that can be observed by comparing the upper

plots of Singh et al. [1] of Figure 3.10 and Figure 3.11, with the lower plots retrieved in the present work of the same figures for 1V.

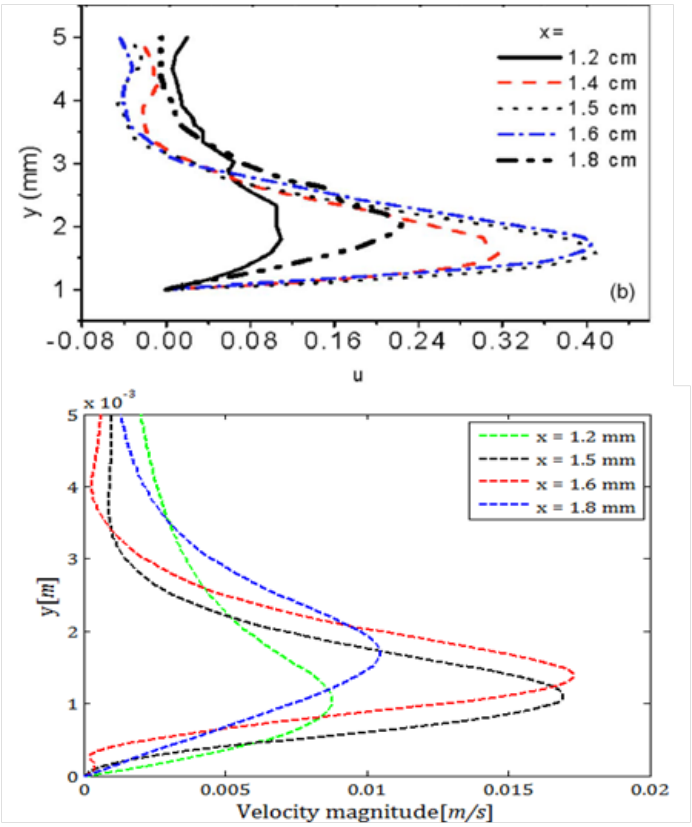

FIGURE 3.11: The normalized velocity components as a function of y for different locations of x, in the upper plot velocity vectors for f =5 kHz and 1000 V retrieved in [1], lower plot velocity vectors for 1 V

3.4 Thrust-Voltage force model assessment

Results of the velocity vectors and velocity profiles for the SDBD force model, Equation 2.6, are simulated. For this case the variables are kept as defined in chapter 2, section 2.2 and 2.3.

From Equation 2.5,

$$\vec{N} = T_{hrust} \times \vec{f}(x,y)_{normalized} \tag{3.9}$$

four different case studies of the thrust, T_{hrust} , are simulated and analyzed,

$$[0.05 \quad 0.1 \quad 0.15 \quad 0.2] \quad N/m$$

Solutions are discuss from lower values to higher values of the thrust.

T=0.05 N/m

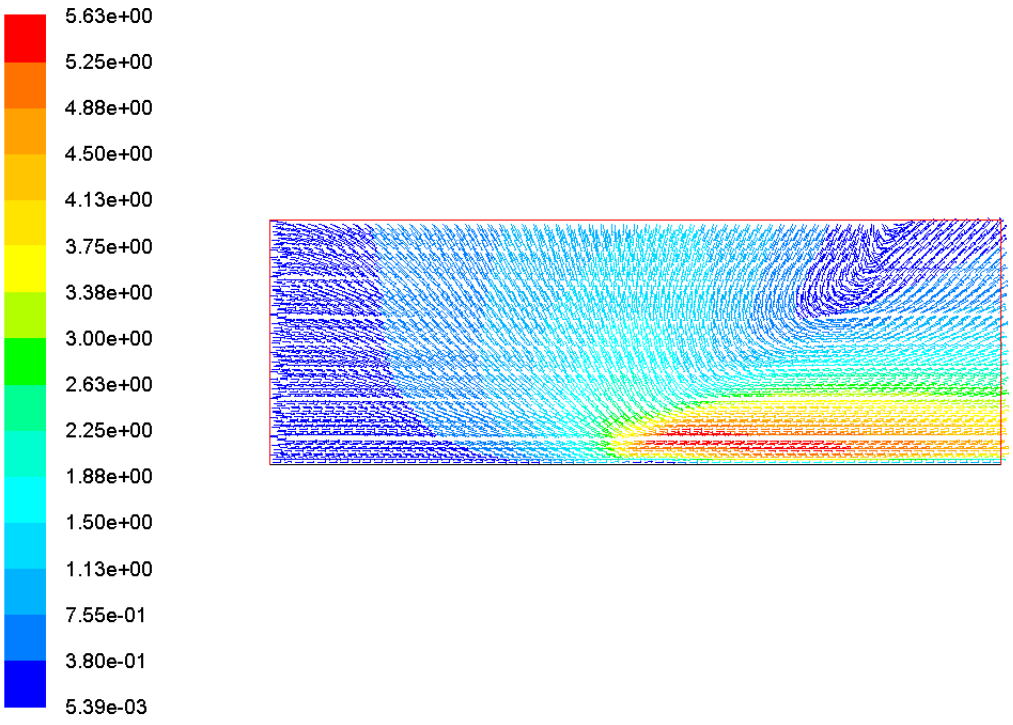

FIGURE 3.12: The velocity vectors for T= 0.05 N/m in m/s

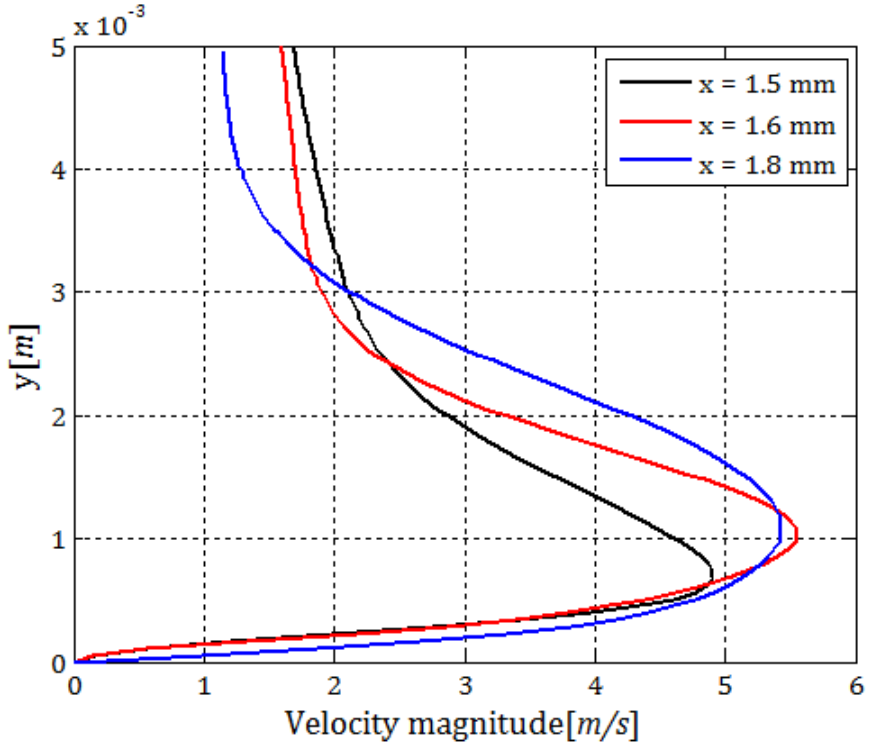

FIGURE 3.13: The velocity vector profiles for three x positions, as a function of y for T= 0.05 N/m

T=0.1 N/m

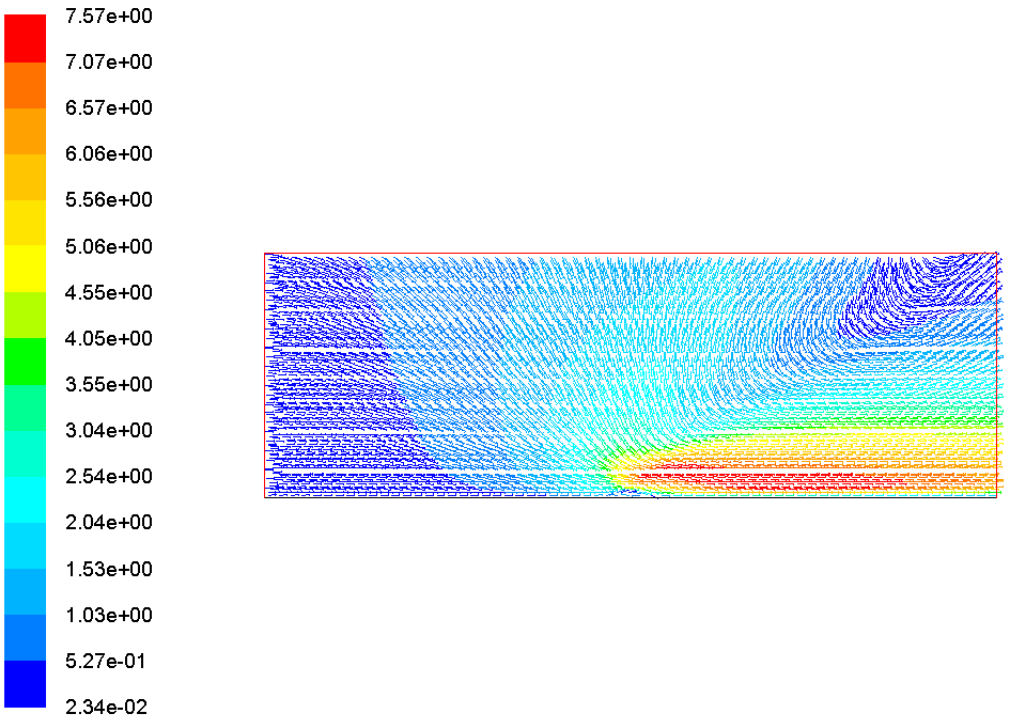

FIGURE 3.14: Velocity vectors for T= 0.1 N/m in m/s

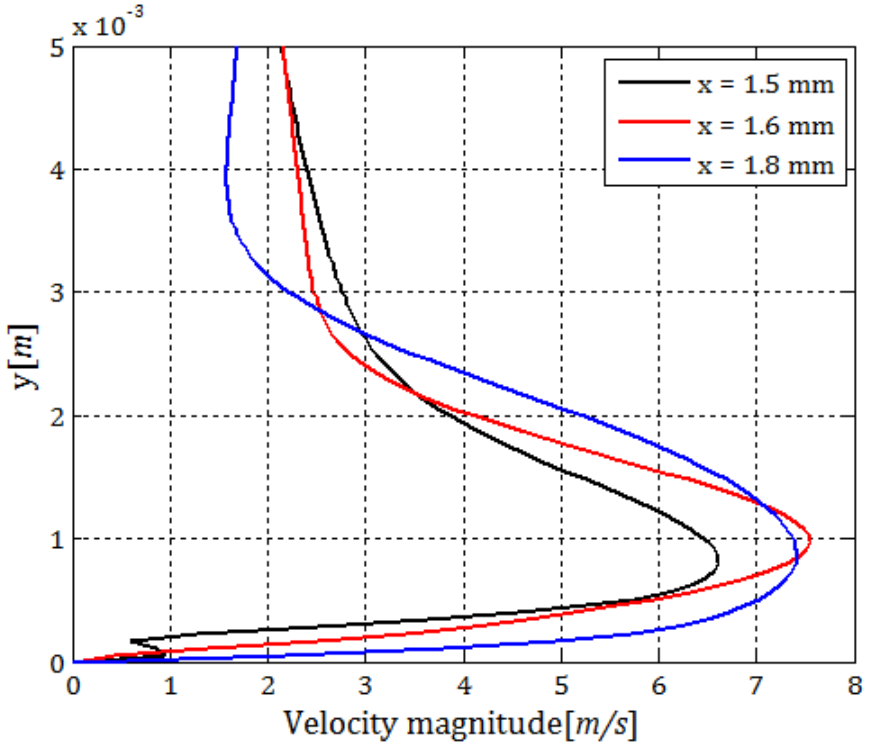

FIGURE 3.15: The velocity vector profiles for three x positions, as a function of y for T= 0.1 N/m

T=0.15 N/m

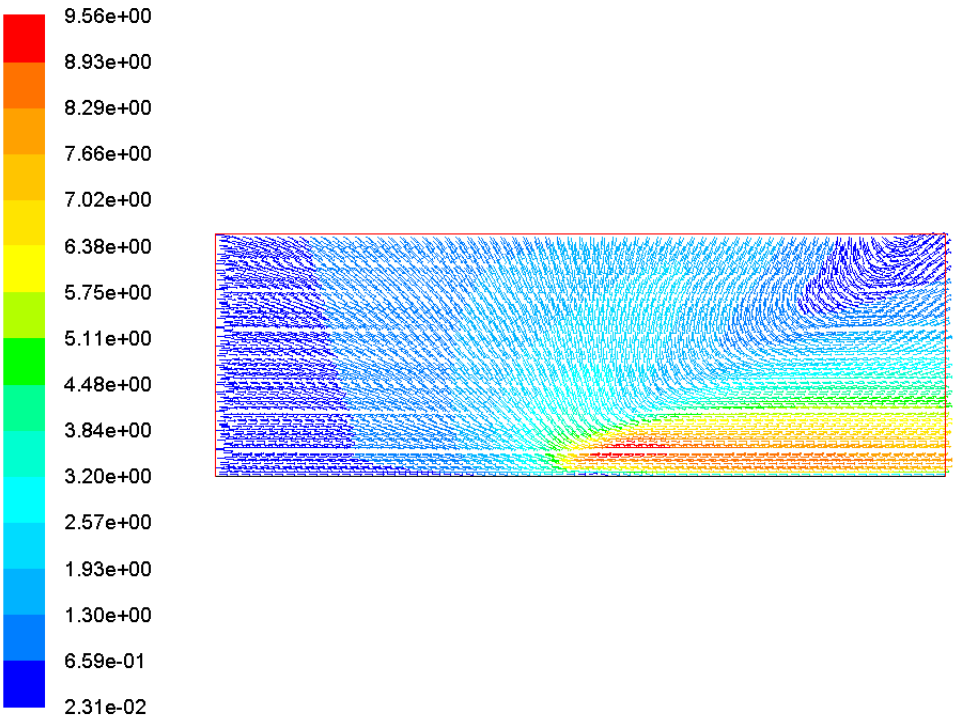

FIGURE 3.16: Velocity vectors for T= 0.15 N/m in m/s

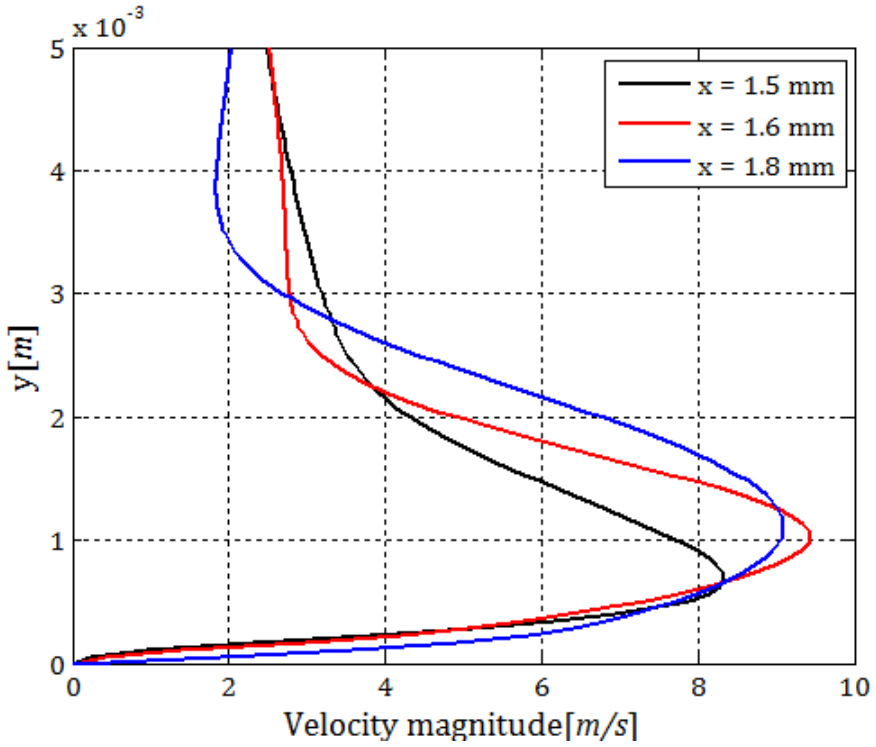

FIGURE 3.17: The velocity vector profiles for three x positions, as a function of y for T=0.15 N/m

T=0.2 N/m

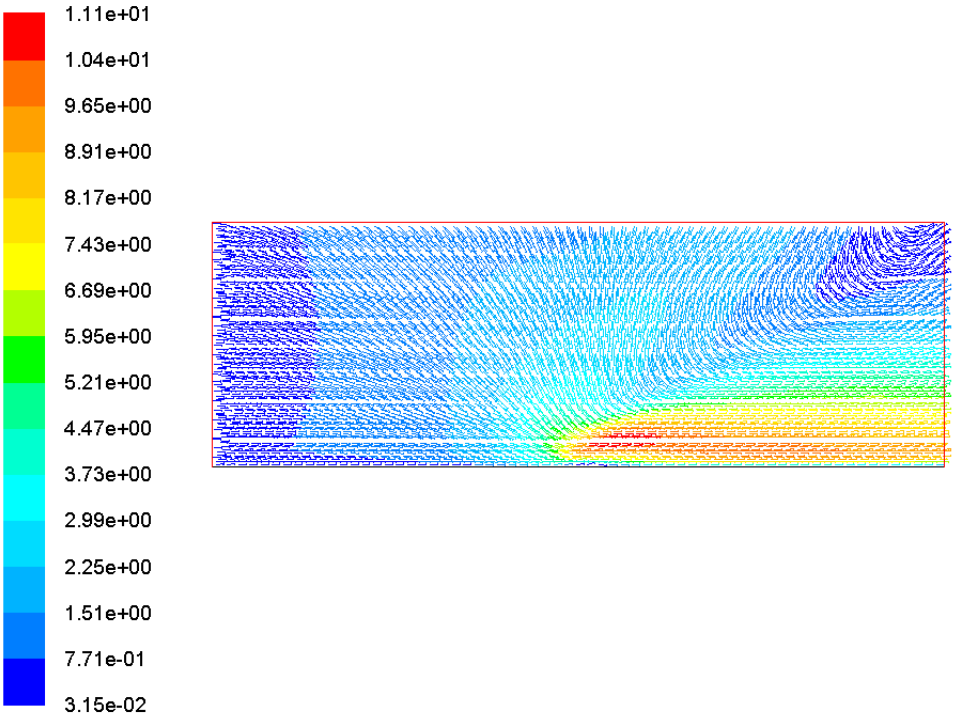

FIGURE 3.18: Velocity vectors for T= 0.2 N/m in m/s

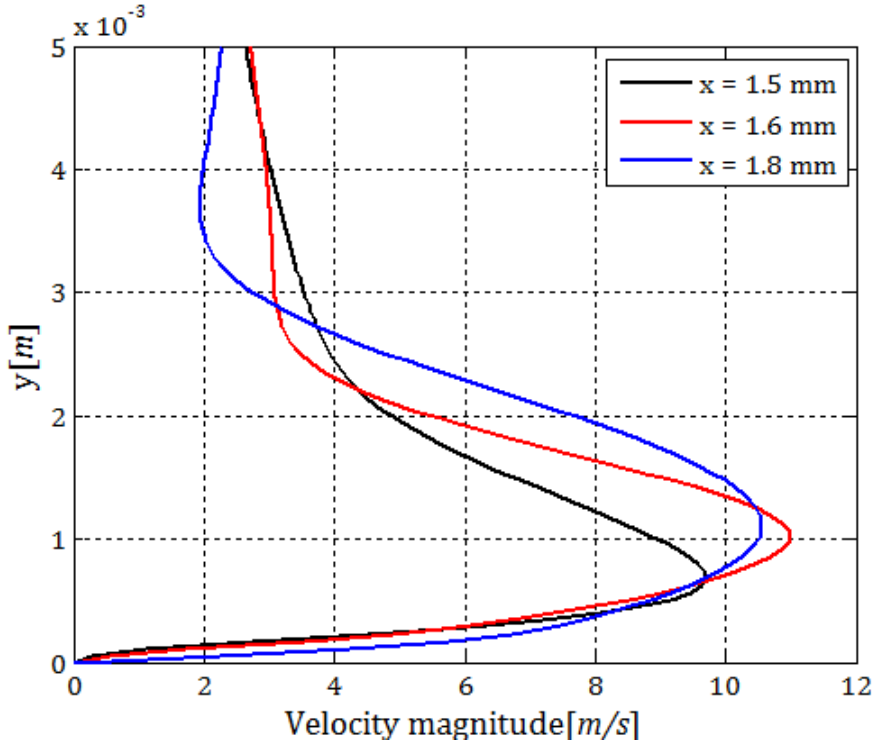

FIGURE 3.19: The velocity vector profiles for three x positions, as a function of y for T= 0.2 N/m

Linear trend of the above solutions is observed. For increasing thrust, the maximum velocity increases too. In addition, there is concordance between the velocity profiles retrieved for the Thrust-Voltage model and the Singh et al. [1] plots, Figure 3.11.

Two agreements can be stated:

- Morphologically agreement with Singh, [1].
- Quantitative agreement of the velocity magnitude with experimental data of [2].

Chapter 4

Voltage-Thrust force model results

Section 3.4 gives a nice relationship between the voltage applied to an SDBD and the velocity magnitude ranges of the surrounding air.

The linear trend noticed in the above section can be sketched resulting into Figure 4.1,

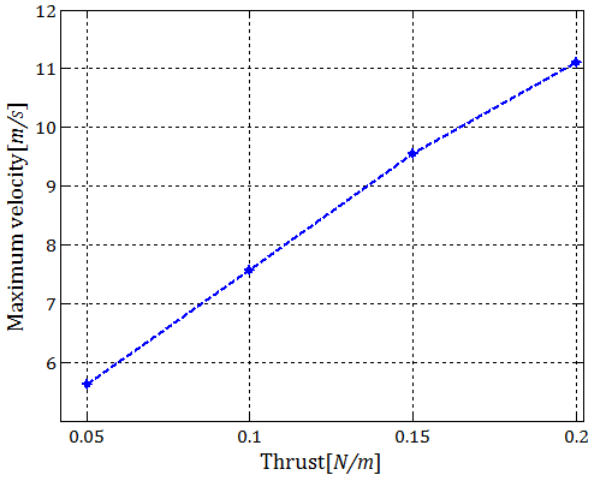

FIGURE 4.1: Thrust versus maximum velocity

In the light of the obtained results, not only the thrust-voltage relation can be sketched, but also the relation between the voltage V_0 and the maximum velocity that can be achieved by an SDBD depending on the material properties and thicknesses.

This last relation comes from combining the Global Thrust model of V R soloviev [5], Figure 2.5, with Figure 4.1, SDBD force model.

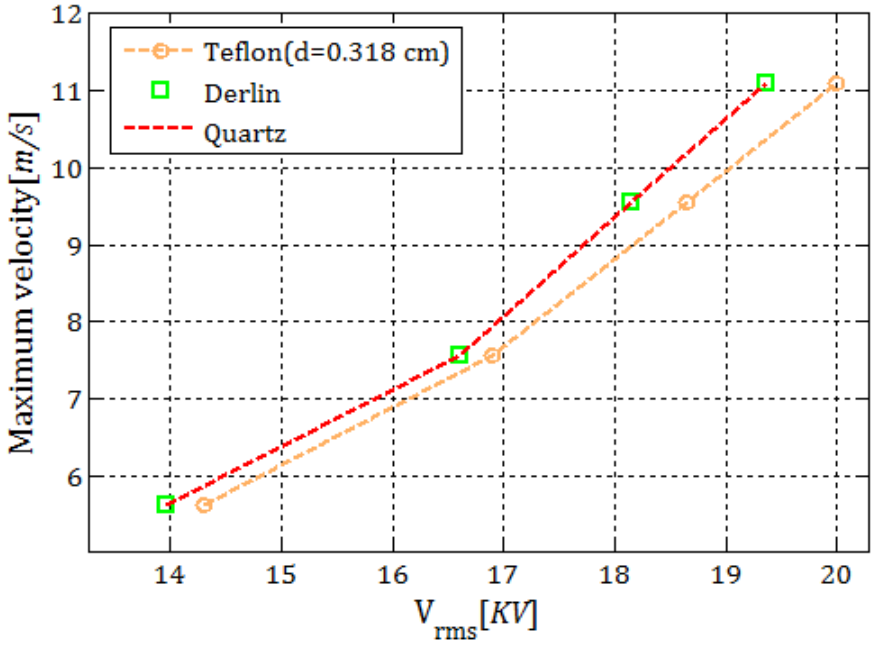

FIGURE 4.2: Voltage to maximum velocity of Teflon, Derlin and Quartz

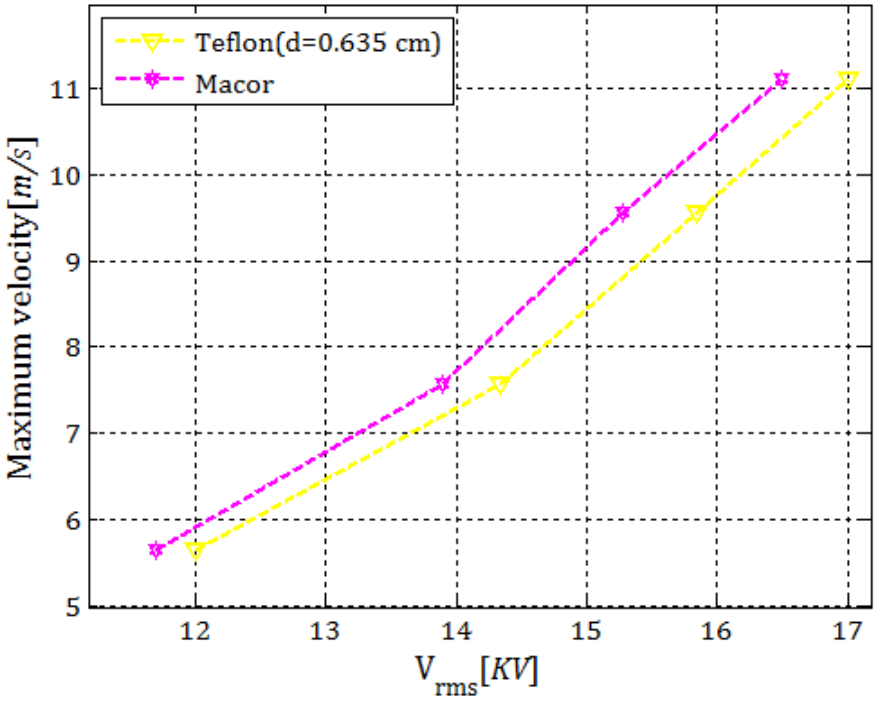

FIGURE 4.3: Voltage to maximum velocity of Teflon and Macor

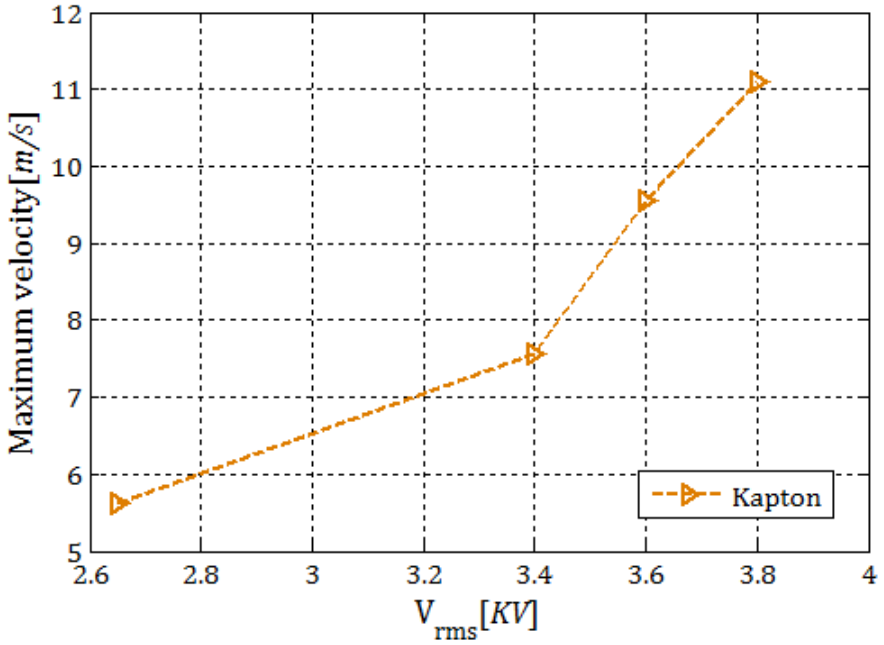

FIGURE 4.4: Voltage to maximum velocity of Kapton

The table gathering all the information for the material properties, thicknesses and the relative dielectric constant for all the above figures is showed hereafter.

Material	d(cm)	$f_v(kHz)$	ε
Teflon	0.635	2.1	2
Derlin	0.635	2.3	3.5
Quartz	0.635	2.3	4.2
Teflon	0.318	2	2
Macor	0.318	2.3	6
Kapton	0.015	4.4	3.9

TABLE 4.1: Material properties

From all the above figures, trends of the maximum velocity versus the voltage have been plot. However, the final analysis of this present work is to compare the numerical results of the maximum velocities with an experimental study, as it is the case of Moreau [2]. Moreau has recently predicted in his work an expression that relates the maximum velocity with the applied voltage, based on a Kapton test as a dielectric material, for SDBD performance. These relation is here presented,

$$U_{max} = 0.000166 \times V^{7/2} \tag{4.1}$$

The plot, showing this predicted exponential behaviour is retrieved from Moreau [2] in the following graph.The results to be analysed correspond to the square marks representing one actuator.

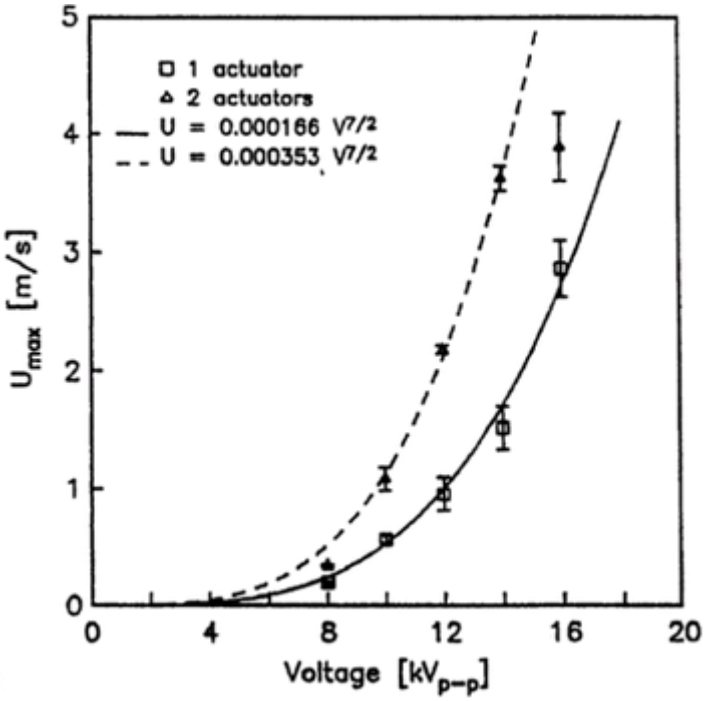

FIGURE 4.5: Moreau estimation of the V_{max} relation with voltage applied using Kapton as dielectric material [2]

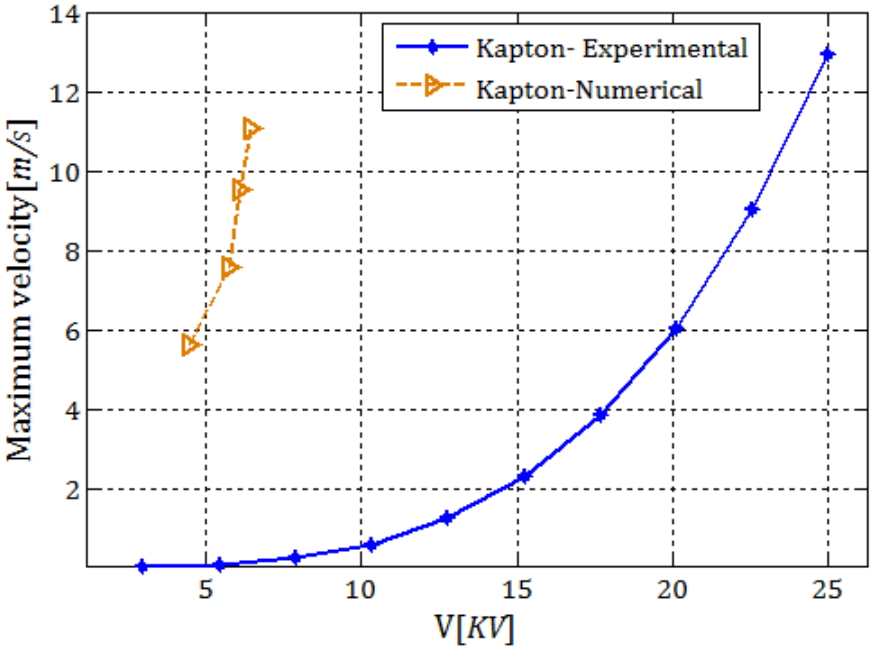

FIGURE 4.6: Experimental data versus numerical data for Kapton

Comparison of the experimental results versus the numerical results of Kapton, Figure 4.6, leads to a concordance in terms of trends of the relation Maximum velocity-Voltage: increasing values of the maximum velocity for higher values of the voltage. However, quantitatively speaking there is no agreement observed, yet within the same order of magnitude. Some of the aspects that should be borne in mind for the differences in the velocity magnitude is that Moreau does not specify the frequency used or the voltage specification: V_0 versus V_{rms} Moreover, in the Thrust- Voltage force model negligible thickness of the electrodes is considered, whereas in [2] plays an important role.

Chapter 5

Socio-economic framework

According to the socio-economic context in which this project is set up, an estimated budget is proposed accounting the fixed and variable costs:

- **Ansys Fluent License.** Software support is needed. Fluent is the CFD program applied, which computes a value of 34,000 €, with a breaking down of costs in:

  -Standalone S/W: 29,000 € -License and updates: 5,500 €

- **Equipment.**Following the next need, a computer is required for the use of the Ansys Fluent products and further mathematical numerical solver such as MATLAB. The approximated price for a computer capable of withstanding the characteristics of these programs is estimated to be 1500 euros.

- **Number of Engineers.**The team can be reduced to two engineers that compare and validate the results.

- **Duration.**The duration of the project,for the proper investigation and analysis of the results is approximated to 6 months, with the collaboration of the two above engineers researchers.

- **Engineer cost per hour.** The engineers are assumed to be paid 30 euros per hour.The working budget with the above data is calculated as follows:

  Total time (T_t) = 300 hours

  Salary $= T_t \times 1$ [engineer] $\times 70$ [euros/hour] $= 21000$ euros

- **Expenditure.** It amounts the variable costs of the electricity among others.

Finally,

Concept	Amount (€)
Ansys Fluent package	34,000
Equipment	1,500
Salary	21,000
Expenditure	300
TOTAL	56,800 €

TABLE 5.1: Cost estimation

On the other hand, the present project is in modeling phase therefore, no related regulations should be addressed till the experimental set up is initiated. Nevertheless, as far as future plasma complications are concerned, it is remarked the main issues that should be taken into account:

- High voltage. High voltage operations need to be carefully controlled.

- Rf unsteady electromagnetic radiation. It can have a detrimental effect on the near communication devices.

- Ozone production. This factor is important in the case the plasma actuator is activated in a close room, as long as ozone is produced in a small proportion during the electrical discharges.

Chapter 6

Conclusions

In the present work the force generated by an SDBD is modeled in to a body source term that can be easily implemented into commercial CFD solver. The motivation of this study is the complexity of the prediction of the thrust generated by a SDBD and its effect on airflow (necessity of coupling the Navier-Stokes equations with Poisson equations and the kinematics) for systematic calculations.

The performed theoretical and numerical calculations with two models of force: global thrust model and local thrust model of a SDBD actuator has led to an interesting force modeling, Thrust-Voltage force model , from an engineering point of view.

The main conclusions regarding the study performed in the present paper are hereafter drawn:

1. Final successful merge of the Soloviev [5] Global thrust model estimation and the Singh et al.[1] Local thrust approximated model. The Thrust-Voltage model provides a full description of the EHD force phenomena, from a qualitatively point of view, in terms of morphology of the velocity profiles, with a proper prediction of the velocity vector profiles, and from a quantitatively point view, in terms of magnitude of the velocity, matching the same order of magnitude of the experimental results.

2. The direct relation between the thrust and the voltage of final SDBD body force expression allows an easy study of the active parameters affecting the plasma actuator. Nevertheless, it is recommended for future lines of study a deeper analysis of the variables coming from the Singh force model, $\vec{f}(F_{x0}, F_{y0}, \beta_x, \beta_y)$.

3. The Thrust-Voltage results on the effect of the maximum velocity have been compared with experimental data of the same dielectric material (Kapton), provided in [2], leading to two main conclusions. The magnitude of the maximum velocity retrieved is higher, yet of the same order of magnitude. Further investigation on this difference can be promising for approaching the model to more realistic data. Nevertheless, there is concordance in terms of the trend of the plotted relation, with increasing velocity for higher voltage.

4. The Voltage-Thrust model allows an easy implementation of the body force into commercial CFD solver, providing time-cost saving in the resolution of problems with SDBD involvement. The decrease of costs comes from the no need of manufacturing an experimental set up for SDBD applications.

6.1 Future lines

Apart from the before mentioned improvements that can be performed to the Thrust-Voltage model in order to approximate it to more realistic data, from this point, many possibilities of study are opened within the aerodynamic scope.

The main driver to keep on working is for boundary layer control of aerodynamic bodies such as UAV, MAV, blades, or airfoils, among others. Which will allow in the future the removal of mechanical moving parts, main cause of vibrational and acoustic problems.

It is left as a future case study, to perform a boundary layer detachment in a numerical simulation and activate the plasma actuator, by means of implementing the body force of the Thrust-Voltage model. Many geometries can be considered from flat plates to NACA airfoil profiles.

Appendix A

Normalization of the local thrust model

The expression to be integrated, and then normalized is equation

$$\begin{aligned}\vec{f}(x,y) = F_{x_0}V_0^4 \exp\left\{-\left(\frac{x-x_0-(y-y_0)}{y}\right)^2 - \beta_x(y-y_0)^2\right\}\vec{i} \\ +F_{y_0}V_0^4 \exp\left\{-\left(\frac{(x-x_0)}{y}\right)^2 - \beta_y(y-y_0)^2\right\}\vec{j}\end{aligned} \tag{A.1}$$

In integral form,

$$\begin{aligned}\vec{F} = \iint r \times \exp\left\{-\left(\frac{x-x_0-(y-y_0)}{y}\right)^2 - \beta_x(y-y_0)^2\right\}\vec{i} \\ + \quad \exp\left\{-\left(\frac{(x-x_0)}{y}\right)^2 - \beta_y(y-y_0)^2\right\}\vec{j} \quad dxdy\end{aligned} \tag{A.2}$$

where $r = \frac{F_{x_0}}{F_{y_0}}$

The value of $V0$ is set to unity as the parameter of the voltage is added from the Equation 2.2. The rest of the values selected so as to solve A.2 are, $F_{x_0} = 2.6$, $F_{y_0} = 2.0$, $x_0 = 0.015$ m, $y_0 = 0.001$ m, $\beta_x = 8 \times 10^5$, $\beta_y = 10^7$.

In order to check the sensibility of the integral to the limits of integration, namely, the area, an study is performed, showing the behavior of the value of the integrated force in modulus, from smaller domains to bigger domains, Figure A.2.

Label	Area $[cm^2]$	Force $[N/m]$
1	0.0002	$\vec{F} = 2.1006 \times 10^{-6}\vec{i} + 1.0585 \times 10^{-6}\vec{j}$
2	0.0015	$\vec{F} = 6.6913 \times 10^{-6}\vec{i} + 1.1707 \times 10^{-6}\vec{j}$
3	0.005	$\vec{F} = 7.4198 \times 10^{-6}\vec{i} + 1.1707 \times 10^{-6}\vec{j}$
4	0.0084	$\vec{F} = 7.4435 \times 10^{-6}\vec{i} + 1.1707 \times 10^{-6}\vec{j}$
out*	0.012	$\vec{F} = 7.4464 \times 10^{-6}\vec{i} + 1.1707 \times 10^{-6}\vec{j}$
out*	0.09	$\vec{F} = 7.4464 \times 10^{-6}\vec{i} + 1.1707 \times 10^{-6}\vec{j}$

TABLE A.1: Force values

* Out of the plotted domain

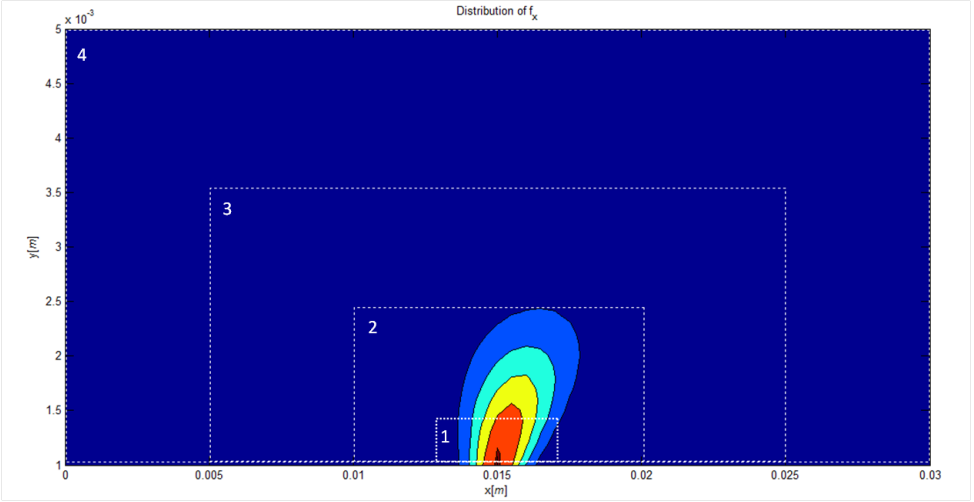

FIGURE A.1: Integration limits

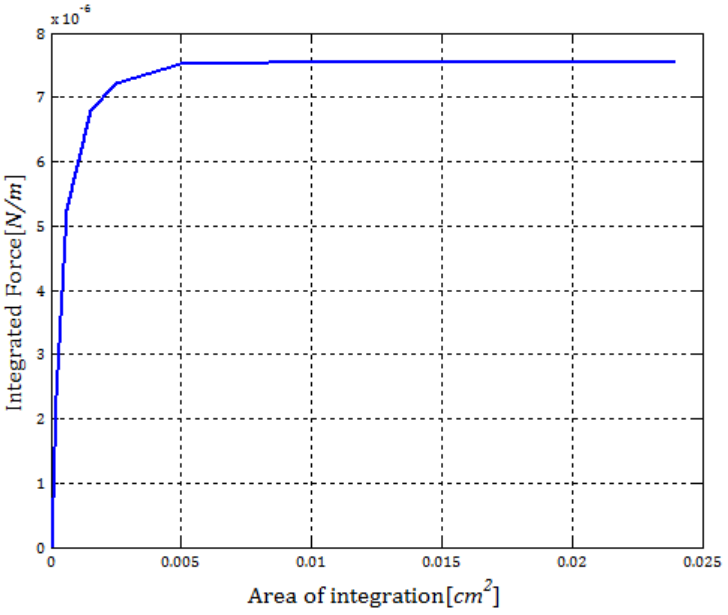

FIGURE A.2: Integration limits

Figures A.1 and A.2 sketch some of the selected areas, from lower rectangles to higher rectangles. Up to the point of 0.01 cm^2 the value where the integral keeps constant.

Then, the final value of the integral taken from the previous results is,

$$\vec{F} = 7.4464 \times 10^{-6}\vec{i} + 1.1707 \times 10^{-6}\vec{j} \tag{A.3}$$

From this point, it remains the task of normalization, consisting in obtaining an expression that fulfills,

$$\frac{\iint \vec{f}(x,y)dxdy}{K} = 1 \tag{A.4}$$

According to the expression A.4, it can be stated that $K = \|\vec{F}\|$. Consequently, K is obtained by means of calculating the modulus of the final value of the integrated force.

$$k = \|\vec{F}\| = \sqrt{(7.4464 \times 10^{-6})^2 + (1.1707 \times 10^{-6})^2} = 7.5359 \times 10^{-6} \tag{A.5}$$

Finally, the distributed force is normalize with respect to K,

$$\vec{f}(x,y)_{normalize} = \frac{\vec{f}\big(F_{x0}, F_{y0}, \beta_x, \beta_y\big)}{\|\vec{F}\|} \tag{A.6}$$

Equation A.6, is the normalized expression of A.1. In order to obtain a final value for the new force model, it is necessary to multiply, the quantitative value of the thrust, namely, the expression of Soloviev [5], equation A.7,

$$T_{sol} = 2.4 \times 10^{-10}{\alpha_l}^4 \frac{fV(cm)}{d(kHz)} \left(\frac{9V_0}{4\Delta V_c}\right)^4 \left(1 - \frac{7\Delta V_c}{6V_0}\right)^4 \left(1 - exp\left(-\frac{1}{4f_v \Delta\tau_q}\right)\right) \tag{A.7}$$

with the expression of the normalized distributed force, equation A.6

$$\vec{T_0} = T_{sol}\big(V, \varepsilon, d, fV\big) \times \frac{\vec{f}\big(F_{x0}, F_{y0}, \beta_x, \beta_y\big)}{\|\vec{F}\|} \tag{A.8}$$

resulting into the final expression A.9,

$$\vec{T_0} = 2.4 \times 10^{-10} {\alpha_l}^4 \frac{f_v(cm)}{d(kHz)} \Big(\frac{9V_0}{4\Delta V_c}\Big)^4 \Big(1 - \frac{7\Delta V_c}{6V_0}\Big)^4 \Big(1 - exp\Big(-\frac{1}{4f_v \Delta\tau_q}\Big)\Big) \times \frac{1}{\|\vec{F}\|} \times \Bigg[r \times \exp\Bigg\{-\Bigg(\frac{x - x_0 - (y - y_0)}{y}\Bigg)^2 - \beta_x (y - y_0)^2\Bigg\}\vec{\imath} + \exp\Bigg\{-\Bigg(\frac{(x - x_0)}{y}\Bigg)^2 - \beta_y (y - y_0)^2\Bigg\}\vec{\jmath}\Bigg] \quad \text{(A.9)}$$

Bibliography

[1] Kunwar Pal Singh and Subrata Roy. Force approximation for a plasma actuator operating in atmospheric air. *Journal of Applied Physics*, 103(1), January 2008. URL http://scitation.aip.org/content/aip/journal/jap/103/1/10.1063/1.2827484.

[2] Eric Moreau. Airflow control by non-thermal plasma actuators. *Journal of Physics D: Applied Physics*, 40(3), 2007. URL http://stacks.iop.org/0022-3727/40/i=3/a=S01.

[3] Y. Babou P. Rocandio, G. Paniagua. Airfoil wake flow modification by means of dielectric barrier discharge. (1), June 2012.

[4] Luigi Barbato. Flow control using dbd plasma actuators: experimental investigation. *Review of Scientific Instruments*, (1), June 2011.

[5] V R Soloviev. Analytical estimation of the thrust generated by a surface dielectric barrier discharge. *Journal of Applied Physics*, 45(2), December 2011. URL http://stacks.iop.org/0022-3727/45/i=2/a=025205.

[6] Jr. Jonh D. Anderson. Fundamentals of aerodynamics. *Boston: McGraw-Hill*, (5th Edition), January 2001.